ISSN (Print) 1226-1750
ISSN (Online) 2233-6656
Journal of Magnetics 19(4), 365-371 (2014) http://dx.doi.org/10.4283/JMAG.2014.19.4.365

The Utility Evaluation of Reconstructed 3-D Images by Maximum Intensity Projection in Magnetic Resonance Mammography and Cholangiopancreatography

Jae-Hwan Cho[1], Hae-Kag Lee[2], Cheol-Soo Park[3], Ham-Gyum Kim[4], Jong-Geun Baek[5], and Eng-Chan Kim[5]*

[1]Department of International Radiological Science, Hallym University of Graduate Studies, Seoul 135-841, Korea
[2]Department of Computer Science and Engineering, Soonchunhyang University, Republic of Korea
[3]Department of Radiological Science, Hallym Polytechnic University, Chuncheon 200-711, Korea
[4]Department of Radiological Technology, Ansan College, Ansan 426-701, Korea
[5]Department of Physics, Yeungnam University, Gyeongsan 705-717, Korea

(Received 14 October 2014, Received in final form 5 November 2014, Accepted 10 November2014)

The aim of this study was to evaluate the utility of 3-D images by comparing and analyzing reconstructed 3-D images from fast spin echo images of MRI cholangiopancreatography (MRCP) images using maximum intensity projection (MIP) with the subtraction images derived from dynamic tests of magnetic resonance mammography. The study targeted 20 patients histologically diagnosed with pancreaticobiliary duct disease and 20 patients showing pancreaticobiliary duct diseases, where dynamic breast MR (magnetic resonance) images, fast spin echo imaged of pancreaticobiliary duct, and 3-D reconstitution images using a 1.5T MR scanner and 3.0T MR scanner were taken. As a result of the study, the signal-to-noise ratio in the subtracted breast image before and after administering the contrast agent and in the reconstructed 3-D breast image showed a high ratio in the reconstructed image of lesional tissue, relevant tissue, and fat tissue. However, no statistically meaningful differences were found in the contrast-to-noise ratio of the two images. In the case of the MRCP image, no differences were found in the ratios of the fast spin echo image and reconstructed 3-D image.

Keywords : breast magnetic resonance image, magnetic resonance cholangiopancreatography, reconstructed 3-D image, signal to noise ratio, contrast to noise ratio

1. Introduction

Due to an increasing westernization of our eating habits and changes of lifestyle, the frequency of breast cancer and pancreaticobiliary duct disease is rising annually. Mammography is known as the most basic and sensitive test for early breast cancer detection and its diagnosis [1-4]. Many tests to diagnose pancreaticobiliary duct diseases exist, but the most common tests are abdominal ultrasonography (US) and abdominal computerized tomography (CT) [5]. However, in the case of mammography, the radiation test is frequently used, and this test lacks the sensitivity and specificity for young women and is not optimal for detecting breast cancer in the transformed breast after surgery [6-8]. US or CT for the diagnosis of pancreaticobiliary duct diseases, especially in the case of bile duct stone, shows different diagnostic accuracies according to the size of stone, the type of stone, and whether the bile duct is expanded or not. Besides this information, common bile duct stones with small sizes are known for having very low diagnostic accuracy [5]. Recently, MRIs have been used to diagnose breast cancer and pancreaticobiliary duct diseases. It is often used as it has excellent image contrast, makes the anatomical evaluation available, and has no risk of radiation exposure. Contrast-enhanced MRIs have been studied and reported to have the highest sensitivity among many other tests [9, 10]. MRI image quality has been improved a lot due to the development of various techniques including 3-D MRI [11]. In addition, MRCP is considered a non-invasive and very accurate image test regarding the bile duct test without the need for exposure to radiation [12]. However, for the existing breast MRI tests, many image tests exist, and many difficulties occur in observing all the images at a glance. Furthermore, with the existing MRCP, it is difficult to obtain the whole picture at once, thus

*Corresponding author: Tel: +82-53-810-2343
Fax: +82-53-810-2343, e-mail: eckim3@hanmail.net

making it tricky to see, for example, whether the pancreaticobiliary duct is narrowed or not, the expansion size of the bile duct, etc. Therefore, a 3-D image is needed to see the whole picture at a glance. When comparing Jang and others' image processing data from 3-D-MRCP and 2-D-MRCP, two cases (4%) were found to have a different anatomic structure, and 15 cases were reported to be helpful when confirming a clear anatomic structure.

When processing images, 3-D-MRCP is able to find hepatic duct bifurcation on the left and right sides by providing a double angle in coronal oblique MIP images with a thickness of slabs [13]. In terms of 2-D breast MRI, since there are many images, it is hard to recreate the locations and interactions of lesions in the breast in one's head. Therefore, by using raw data, this study creates 3-D restructured images of a Three-Dimensional Shaded-Surface (3-D SSD) and uses the Maximal Intensity Projection technique (MIP). These 3-D images not only help doctors treat their patients but also distinguish contrast enhanced lesions from small blood vessels [14, 15]. With 3-D MIP, it is possible to produce 3-D images using already existing contrast-enhanced MRI images. Also, we can confirm the location of the lesion with enhanced contrast through a 3-D image. Accordingly, in the present study, we tried to determine the utility of 3-D images by comparing and analyzing the reconstructed 3-D images from fast spin echo of MRCP using MIP with the subtraction image achieved by performing the dynamic test of breast MRIs.

2. Subjects and Method

2.1. Study subjects

Between March 2010 and December 2010, 20 patients with a malignant tumor size bigger than 10 mm^3 were selected among patients diagnosed with histological Ductal Carcinoma In Situ (DCIS). Since the sizes of malignant tumors were mostly over 1.0 cm, the study was conducted with patients who had a size of tumor over 10 mm^3 [16]. Besides these patients, we also targeted 20 patients showing bile duct expansion among patients with pancreaticobiliary duct diseases out of the patients undergoing abdominal US for further accurate analysis. The age of breast cancer patients ranged from 39 to 58 years with an average age of 43.7 years. Patients with radiation therapy or neoadjuvant chemotherapy before treatment and before MRI performance were excluded. The age of pancreaticobiliary duct patients ranged from 52 to 72 years with an average of 62.8 years. Patients with chronic hepatitis, cirrhosis, and fatty liver but no expansion of bile duct were excluded from the survey list.

2.2. Data acquisition

We used a 3.0T MR scanner (GE Healthcare. Milwaukee. WI, USA) and HD T/R 8ch breast array coil (In vivo Corp. Gainesville. FL, USA) to get the breast MR images as well as a phased array multi-coil. To get MRCP images, we used a 1.5T MR scanner (Signa 1.5T HDx. GE Healthcare. Milwaukee. WI, USA) and HD T/R 8ch Torso array coil (In vivo Corp. Gainesville. FL, USA) including a phased array multi-coil. To produce dynamic breast MR images, we got the cross-sectional image before enhancing the contrast and four images after enhancing contrast using the VIBRANT 3-D method. First, after getting the image before administration of the contrast agent, we got four cross-sectional images while the infusion of 0.5 mmol/ml gadodiamide contrast agent was injected in the patients. The image variables were as follows:

TR: 9 ms; TE: 4.25 ms; Matrix: 512×320; NEX: 1; Slice thickness: 20 mm; FOV (field of view): 320 mm; flip angle: 10^0

We got four images during the transverse relaxation image, which was obtained before and after enhancing contrast using the achieved volume image breast assessment (VIBRANT) 3-D to indicate which version of the Advantage Windows workstation was used.

We produced an image after subtracting the image we got before administering the contrast agent, and the image with highest contrast level among the breast cancer site and its surrounding tissues out of the four images sent to Advantage Workstation (Fig. 1).

Next, we obtained the images on the axial plane, a T2 enhanced image using respiratory-triggered and fat saturation methods through fast spin echo test in the MRCP image.

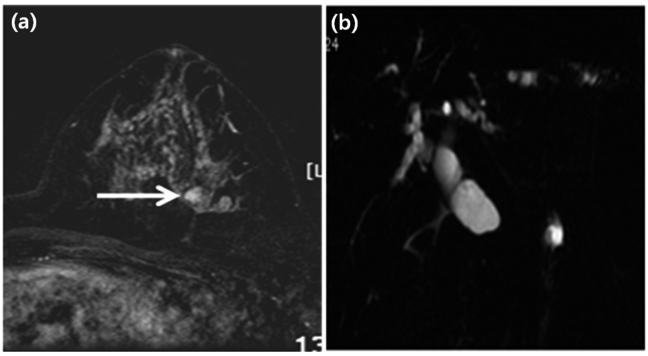

Fig. 1. We obtained the image with high contrast and the image treated after subtracting the image before administration of the contrast using transverse relaxation enhanced image before and after enhancing contrast agent by achieved VIBRANT 3-D method (a). Next, we obtained the image on the axial plane, T2 enhanced image using the respiratory-triggered method and fat saturation method by fast spin echo method in MRCP image (b).

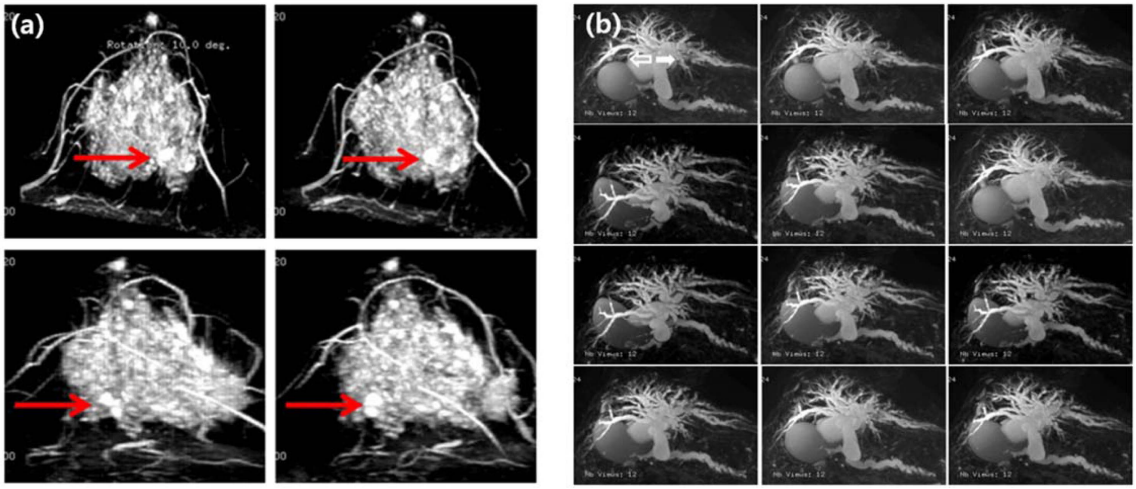

Fig. 2. (Color online) We obtained the reconstructed 3-D image with a 10- mm thick cut layer using MIP and turning the image (b) achieved using the fast spin echo method in the subtracted breast image (a) and MRCP image to the left and to the right at a 15 degree angle.

The image variables were as follows (Fig. 1).

TR: 3000 m; TE: 560 ms; Matrix: 320×224; NEX: 2; Slice thickness: 14 mm; FOV: 359 mm

2.3. Image reconstruction

We achieved our 3-D reconstructed image by turning to the left and to the right with a 100-mm thick cut layer and at the angle of 15 degrees when handling the image obtained through the subtracted image of the breast and fast spin echo of MRCP image using MIP (Fig. 2). MIP is one of the most popular projection shading methods and is also one type of rendering methods widely used in the field of CT or MRI angiography. MIP rendering is the rendering method where we determine the highest density following the volume ray applicable to CT but not for MRI, and it considers the highest density value on the ray as in Eq. (1) as the final output pixel value instead of the volume ray integration.

$$I = \max(s(x(\lambda))),\ (0 < \lambda < D) \tag{1}$$

The basic principle is that we perform rendering while choosing voxels with the strongest signal after removing the voxels with low-strength signals lying on the line by penetrating the structures through the 2-D image accumulated along the Z-axis. The original MIP approach simply projects the maximum scalar value along a sampling ray from the eye through a pixel. Eq. (1) defines the operation applied to a scalar function $f(z)$, defined on a sampling ray through pixel p and parameterized by z. Typically, the resulting scalar value is converted to a grey level intensity. Herein, we limit the ray depth to a distance D extending from the image plane to a distance past where the ray exits the volume [11]. MIP involves a search over all values on a ray and, thus, is an expensive operation. Also, the selection operation ignores visibility ordering as well as depth information so that higher valued structures farther away may occlude portions of closer structures. Interpretation of such a MIP computed image can be difficult without such cues. A variation to MIP [17, 18] applies depth shading to the original MIP approach with a weight function parameterized by distance from the eye. We call this approach DMIP and illustrate its operation in Eq. (2).

$$I(p) = \max_{0 \le z \le D}(f(z)) \tag{2}$$

Heidrich *et al.* [17, 18] used standard graphics hardware and a linear function for $d(z)$. A later variation to MIP, called LMIP, finds the closest local maximum greater than a user-defined threshold. Eq. (3) defines the LMIP operation with a threshold t, where LMAX is true if the function value is a local maximum.

$$I(p) = \max_{0 \le z \le D}(d(z) \cdot f(z)),\ 0 \le d(z) \le 1 \tag{3}$$

If no scalar on the ray is greater than or equal to t, then the maximum intensity is projected as in the original MIP approach. Implementations using front-to-back ray traversal can exploit early ray termination for this particular technique. The application of classification 9 using transfer function g can help to pick, remove, or contrast-enhance various structures. A transfer function is defined as any function which returns some material property. We consider transfer functions that modulate the scalar field. As

shown in Eq. (4), the maximum operation is applied to the transformed scalar value.

$$I(p, t)=f(z_k),\ z_k=\max_{0\le z\le D}(z\backslash((f(z)\ge t)\ \text{AND LMAX}(z))) \tag{4}$$

Examples of some commonly used transfer functions are ramp, step, and window functions although the function may be defined arbitrarily. One example of the use of a transfer functions in data for medical visualization is to window value ranges that represent particular tissue types. This example is shown in Eq. (5).

$$I(p) = \max_{0\le z\le D}(gf(z)) \tag{5}$$

2.4. Image evaluation

Next, the subtracted image of the breast, where the image is retrieved from the fast spin echo method in the MRCP image, and the reconstructed 3-D image, where we measure the signal intensity at the same site. From the measured site of the breast image, the ROI was located at the end of one side of the breast site with the lesion to measure the central part of the lesion, the surrounding relevant tissues, and the fat tissues. The size of this area of interest was 15 mm^2. For the measured site of the MRCP image, the ROI was located in three sites: the hepatic duct part, the central part of the gallbladder, and the common bile duct area. The size of this area of interest was 10 mm^2 (Fig. 3). The size of the ROI was automatically set to 10 mm^2 and located to the anatomic area of interest. For the quantitative analytic method of the breast image, we obtained the signal-to-noise ratio of the area of interest in the two images and averaged them. Based on the signal-to-noise ratio of the lesion, we determined the contrast-to-noise ratio of each area of interest and averaged them. Finally, we compared and analyzed the figures in the two images. For the signal-to-noise ratio, we divided the signal strength value of the central part of the lesion, its relevant tissue, and fat tissue with the signal strength value of the background standard deviation. In the case of the contrast-to-noise ratio of the lesion, we determined its value by dividing the difference between the signal strength of the lesion and that of the fat tissue with the signal strength of the background standard deviation. For the contrast-to-noise ratio of the relevant tissue, we determined its value by dividing the difference between the signal strength of the relevant tissue and that of the fat tissue with the signal strength of the background standard deviation. To show the background standard deviation, we measured it at the top left part of the breast and the bottom right of the breast in the phase encoding direction and showed its average and its standard deviation. For the quantitative analytic method for the MRCP image, we determined the signal-to-noise ratio of the area of interest in the fast spin echo image and the reconstructed 3-D image of the fast spin echo image and averaged them. Based on the signal-to-noise ratio of the gallbladder, we determined the contrast-to-noise ratio of each part of interest, obtained their average, and compared and analyzed the figures of the three images. In terms of signal-to-noise ratio, we divided the signal strength value of the central part of the gallbladder and of both the front and rear areas 15 mm away from the central part of the gallbladder with the signal strength value of the background standard deviation just like Eq. (6). For the contrast-to-noise ratio, we divided the difference of the signal strengths between gallbladder and the other area of interest with the signal strength value of the background standard deviation. For the background standard deviation, we measured it at the top left and bottom right of the abdominal surface in the phase encoding direction and presented it as the average and the standard deviation. The equations to get the signal-to-noise ratio and the contrast-to-noise ratio applied in this study are as follows:

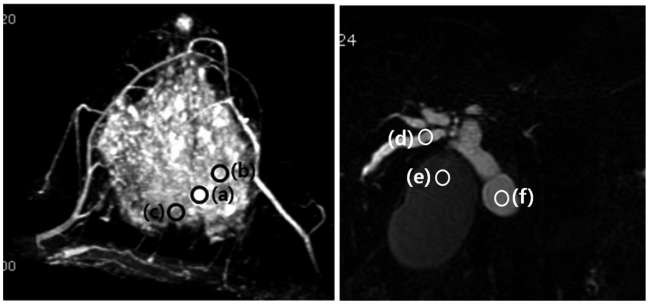

Fig. 3. For the measured site of the breast image, ROI was located at the one end part of the breast with the lesion to measure the central part of the lesion (a), the relevant tissue, the surrounding tissue (b), and the fat tissue (c). For the measured part of MRCP image, ROI was located at the three parts including the hepatic duct part (d), the central part of gallbladder (e), and the common bile duct part (f).

$$\text{SNR} = \frac{\text{SI(region, surrounding tissues)}}{\text{SDN}} \tag{6}$$

SNR: signal to noise ratio
SDN: standard deviation of noise in the background
SI: signal intensity

$$\text{CNR} = \frac{\text{SI(region)} - \text{SI(surrounding tissues)}}{\text{SDN}} \tag{7}$$

CNR: contrast to noise ratio

SDN: standard deviation of noise in the background
SI: signal intensity

2.5. Statistical analysis

To get the difference in the average values of the signal-to-noise ratio and contrast-to-noise ratio, the paired student t-test (SPSS win 16.0, USA) was used, and a statistically meaningful difference was only considered in the case of a P value less than 0.05.

3. Results

As a result of the quantitative analysis, the signal-to-noise ratio of the lesion was 12.74 ± 3.39; that of the relevant tissue was 6.35 ± 3.12; and that of the fat tissue was 2.34 ± 1.15. All values were for in the breast image undergoing subtraction before and after administering the contrast. In the case of the contrast-to-noise ratio, the contrast-to-noise ratio of the lesion was 2.32 ± 0.14, and that of the relevant tissue was 2.39 ± 1.65. For the reconstructed 3-D image, the signal-to-noise ratio of the lesion was 15.21 ± 3.86; that of the relevant tissue was 7.24 ± 3.21; and that of fat tissue was 3.22 ± 2.01. The contrast-to-noise ratio of the lesion was 2.27 ± 1.149, and that of the relevant tissue was 2.53 ± 1.76 (Table 1). The signal-to-noise ratio of the lesion, relevant tissue, and fat tissue in the subtracted image before and after administering the contrast and the reconstructed 3-D image showed the highest level signal-to-noise ratio in the reconstructed image. No big difference for the average in the contrast-to-noise ratio of the two images ($p < 0.05$) occurred (Fig. 4). For the MRCP image using the FSE method, the signal-to-noise ratio of the transhepatic duct was 12.25 ± 2.29; that of the gallbladder was 6.24 ± 1.43, and that of the common bile duct was 14.13 ± 0.27. For the reconstructed 3-D image of the FSE image, the signal-to-noise ratio of the transhepatic duct was 11.77 ± 2.28, and that of the gallbladder was 6.72 ± 2.43; that of the common bile duct was 13.98 ± 3.33 (Table 2). These results mean that no difference in the signal-to- noise ratio in the fast spin echo image and the reconstructed 3-D image of the fast spin echo image in three parts occurred ($p > 0.05$) (Fig. 5). The contrast-to-noise ratio of the transhepatic duct was 3.02 ± 2.11 in the fast spin echo image, and that of the common bile duct was 2.73 ± 1.31. For the reconstructed 3-D image of the fast spin echo image, the contrast-to-noise ratio of the transhepatic duct was 2.98 ± 1.22, and that of the common bile duct was 2.73 ± 1.02 (Table 2). The contrast-to-noise ratio of the transhepatic duct and the common bile duct did not show any statistically

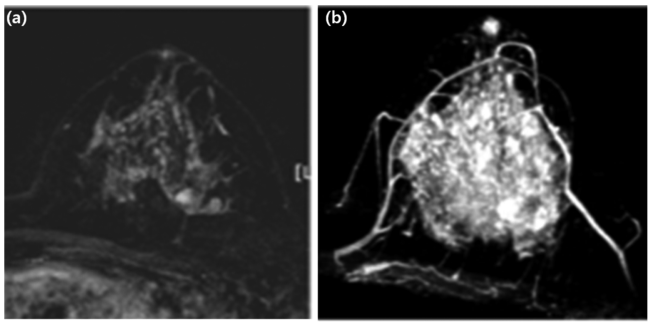

Fig. 4. The breast image subtracted before and after administering the contrast agent and the reconstructed 3-D breast image.

Table 1. Signal to noise ratio and contrast to noise ratio in the breast image subtracted before and after administering contrast agent and the reconstructed breast 3-D image.

Group	SNR			CNR	
	Lesion	Relevant tissue	Fat tissue	Lesion	Relevant tissue
Subtraction image	12.74 ± 2.39	6.35 ± 3.12	2.34 ± 1.15	2.32 ± 0.14	2.39 ± 1.65
Reconstructed 3-D image	15.21 ± 3.86	7.24 ± 3.21	3.22 ± 2.01	2.27 ± 1.149	2.53 ± 1.76

SNR: signal to noise ratio, CNR: contrast to noise ratio

Table 2. Signal to noise on the SSFSE, FSE, and Reconstruction images.

group	SNR (Mean ± SD)			CNR (Mean ± SD)	
	HD	GB	CBD	HD	CBD
FSE	12.25 ± 2.29	6.24 ± 1.43	14.13 ± 0.27	3.02 ± 2.11	2.73 ± 1.31
Reconstruction image	11.77 ± 2.28	6.72 ± 2.43	13.98 ± 3.33	2.98 ± 1.22	2.73 ± 1.02
p	0.07	0.052	0.065	0.06	0.055

SNR: signal to noise ratio, CNR: contrast to noise ratio, HD: hepatic duct, GB: gallbladder, CBD: common bile duct, SSFSE: single shot fast spin echo, FSE: fast spin echo, SD: standard deviation
Interaction effect using an paired T test

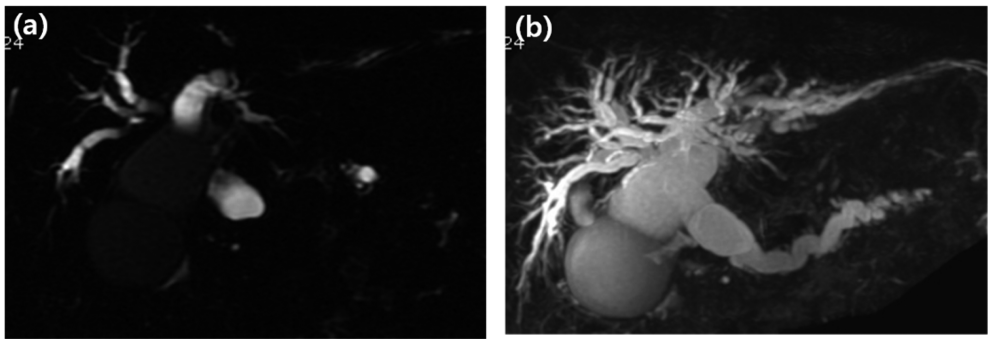

Fig. 5. T2 weighted image using the respiratory-triggered and fat saturation methods in FSE imaging (B) and reconstruction image of FSE image with MIP (C). SNR is higher in the FSE image and reconstruction image compared to the SSFSE image and was not different between the FSE image and reconstruction image.

meaningful difference ($p > 0.05$).

4. Discussion

Breast MRIs are reported to diagnose breast cancer more precisely and predict size more accurately as it judges the lesion by combining the morphological standard and the result of the dynamic contrast enhancing making it different from mammography or breast ultrasonography [19, 20]. In addition, MRCP shows excellent diagnostic sensitivity and specificity in the evaluation of the pancreaticobiliary duct and in the diagnostic of pancreaticobiliary duct diseases, it is carried out prior to Endoscopic Retrograde Cholangiopancreatography (ERCP) [12].

Furthermore, it is a non-invasive test and provides projection and cross sectional images of the pancreaticobiliary duct system with good quality and without oral or venous contrast agent administration. In addition, it is also possible to evaluate the lesions of the other areas excluding the gallbladder. Besides this, it has low examiner dependence, and it also avoids exposure to ionized radiation [12]. However, so many existing tests exist so that the help of a 3-D image is needed to get the whole picture from any images at first glance. In this study, we produced 3-D images using MIP. In 3-D MIP, we first obtained the source image and showed the image after choosing the pixels with the highest signal strength and, thereafter, reconstructing them. This technique is usually used for blood vessel tests. Korogi *et al.* [21] reported that the blood vessel image obtained from the 3-D MIP shows more than 85% sensitivity and almost 100% specificity for the diagnosis rate of occlusive vascular disease. Willinek *et al.* [22] reported that they obtained images through 3-D MIP using contrast agent and could get blood vessel images of high resolution and contrast charts with good quality. Kim and his colleagues [23] compared the diagnostic efficiency of a single shot fast spin echo with that of a 3-D fast spin echo targeting patients with gallbladder stones. They reported that there was no difference in the accuracy of diagnosing the gallbladder stone, but the diagnostic range could be broadened as the spatial location could be confirmed using the reconstructed 3-D image. In this study, we examined the breast test and pancreaticobiliary duct test while applying the methods usually used in blood vessel tests. As a result of the study, the signal-to-noise ratio of the subtracted image before and after administering contrast agents and the reconstructed 3-D image showed a high signal-to-noise ratio in the reconstructed image of the lesion, the relevant tissue, and the fat tissue. However, the contrast-to-noise ratio of the two images did not show a statistically meaningful difference. The quality level of the two images can be considered similar. However, we confirmed that the reconstructed 3-D image can give the same information as the 3-D image. Kim *et al.* [24] reported that they studied the diagnostic efficiency of the lesion regarding the achieved image using 3-D MIP, and as a result, they could find malignant multifocal lesions that could not be found in 2-D images. The study excluded research about the diagnostic effectiveness of the lesion's discovery rate, but a 3-D-MRCP image could be evidence for clear anatomic structure. The MRCP study did not show any difference between the signal-to-noise ratio and contrast-to-noise ratio in the reconstructed 3-D image of the fast spin echo image, which could be considered to support the results of the study carried out by Kim and his colleagues. This study had several limitations. First, it was difficult to assign an area of interest because of the difference between the 2-dimensional images and reconstructed 3-dimensional images. Second, the signal intensity was different depending on the patients' characteristics. Therefore, it was not measured under identical conditions. Third, the number of

patients was too low to make a definitive conclusion. Therefore, further study with a larger cohort will be needed.

5. Conclusion

During the performance of breast contrast tests and MRI pancreatic duct contrast tests, 3-D images using MIP provided excellent information about the number, shape, and location of the lesions, and this technique is expected to give proper information for diagnosis as it gives an image with high signal strength.

Acknowledgments

Jae-Hwan Cho and Hae-Kag Lee equally contributed to this work. They are co-first authors. “This work was supported in part by the Soonchunhyang university Research Fund”.

References

[1] C. K. Kuhl, S. Schrading, C. C. Leutner, N. Morakkabati-Spitz, E. Wardelmann, R. Fimmers, W. Kuhn, and H. H. Schild, J Clin Oncol. **23**, 8469 (2005).
[2] H. L. Carol, Radiol. Clin. N. Am. **40**, 395 (2002).
[3] E. A. Morris, Semin Roentgenol. **36**, 226 (2001).
[4] R. W. Katzberg, Invest Radiol. **29**, 94 (1994).
[5] J. K. Lee, P. L. Rhee, and J. H. Lee, Korean J. Gastroenterol. **29**, 85 (1997).
[6] S. G. Orel, M. G. Hochman, M. D. Schnall, C. Reynolds, and D. C. Sullivan, Radiographics. **16**, 1385 (1996).
[7] E. A. Morris, Radiol. Clin. North. Am. **40**, 443 (2002).
[8] L. A. Carbonaro, F. Pediconi, N. Verardi, R. M. Trimboli, M. Calabrese, and F. Sardanelli, AJR. Am. J. Roentgenol. **196**, 942 (2011).
[9] J. A. Jesberger, N. Rafie, J. L. Duerk, J. L. Sunshine, M. Mendez, S. C. Remick, and J. S. Lewin, J. Magn. Reson. Imaging **24**, 586 (2006).
[10] S. Kul, A. Cansu, E. Alhan, H. Dinc, G. Gunes, and A. Reis, AJR Am. J. Roentgenol. **196**, 201 (2011).
[11] M. Friedrich. Eur. Radiol. **8**, 707 (1998).
[12] B. K. Wallner, K. A. Schumacher, and W. Weidenmer, Radiology **181**, 805 (1999).
[13] J. K. Jang, D. G. Seo, and Y. J. Kim, Journal of The Korean Society of MR Technology **24**, 199 (2014).
[14] B. L. Daniel, K. L. Granlund, C. J. Moran, M. T. Alley, J. Lipson, D. M. Ikeda, J. Kao, and B. A. Hargreaves, Eur. J. Radiol. **81**, S24 (2012).
[15] E. A. Morris, and L. Liberman, FACR. Breast MRI: Diagnosis and Intervention. Springer, 2005.
[16] J. M. Chang, W. K. Moon, N. Cho, W. Han, D. Y. Noh, I. A. Park, and E. J. Jung, Eur. Radiol. **20**, 1093 (2010).
[17] S. Naeem and C. Roger, Crawfis. Proc. SPIE **4665**, 13 (2002).
[18] W. Heidrich, M. McCool, and J. Stevens, Proc. IEEE Vis. **95**, 11 (1995).
[19] E. S. Cha, J. Breast. Canc. **6**, 247 (2003).
[20] T. Hata, H. Takahashi, K. Watanabe, M. Takahashi, and K. Taguchi, Itoh. T. Am. Coll. Surg. **198**, 190 (2004).
[21] Y. Korogi, M. Takahashi, and T. Nakagawa, AJNR **18**, 135 (1999).
[22] W. A. Willinek, J. Gieseke, and R. Conrad, Radiology **25**, 583 (2002).
[23] J. A. Kim, E. J. Yun, and S. C. Choi, J. Korean Radiol. Soc. **54**, 97 (2006).
[24] H. S. Kim, B. J. Kang, and S. H. Kim, Korean Soc. Magn. Reson. Med. **13**, 183 (2009).